CORRELATION BETWEEN EVA DEGREE OF CROSSLINKING AND MOISTURE INGRESS INTO PV LAMINATES

Djamel Eddine Mansour[1], Stefan Mitterhofer[2], Christoph Herzog[1], Esther Fokuhl[1], Marko Jankovec[2], Paul Gebhardt[1], Daniel Philipp[1]
[1] Fraunhofer Institute for Solar Energy Systems ISE, Heidenhofstrasse 2, 79110 Freiburg im Breisgau, Germany
+49-761-4588-5880
[2]Faculty of Electrical Engineering, University of Ljubljana, 1000 Ljubljana, Slovenia
djamel.eddine.mansour@ise.fraunhofer.de
https://www.ise.fraunhofer.de

ABSTRACT: The degradation of a PV module is strongly influenced by moisture ingress. Previously most of the investigations of the diffusion properties of encapsulants and backsheets were carried out on the polymer sheets alone, and thereby not accounting for diffusion properties of all involved materials. In this work, the kinetic study of the water uptake of the EVA was performed inside the laminate stack, using incorporated miniature digital humidity sensors at different EVA depths. Samples with different polymeric materials and lamination conditions were aged under a damp-heat (DH) and UV/DH (combined) conditions while applying an in-situ moisture monitoring technique for PV modules. From this data, we calculated the respective diffusion rates and determined how the different materials and lamination conditions affect the mechanism of moisture ingress/egress during the aging tests. The results demonstrate a faster diffusion in the CPC backsheet than in the TPT backsheet type. With respect to the lamination process, the effective activation energy (E_A^{eff}), calculated assuming an Arrhenius-like behavior showed slower moisture ingress for the shortly laminated sample. Furthermore, the effect of the UV irradiation on the diffusion behavior during the combined UV-DH aging test is presented.
Keywords: Encapsulant, backsheet, moisture ingress / egress, humidity sensors, damp-heat (DH) exposure, UV-DH combined aging

1 INTRODUCTION

Ingress of moisture into PV modules has a major influence on the long-term reliability. The influence of poorly crosslinked EVA on the moisture ingress of PV modules has been investigated [1,2] . Discoloration has been observed at soldering ribbons on modules with short lamination times upon accelerated aging [3], which is a strong indication for moisture ingress as a main driver of corrosion [4,5]. The diffusion properties are determined by the polymeric layers (backsheet and encapsulant) which both have only a partial moisture barrier. In the case of ethylene vinyl acetate (EVA) encapsulants, moisture can react at elevated temperatures with the VA content, forming acetic acid which then reacts with the metallic components of the cells, causing corrosion [6].

In order to predict the moisture ingress into the PV modules, different theoretical models have been proposed: e.g. via Finite Element Analysis (FEA) for the prediction of the moisture content in the laminate structures based on the Fickian diffusion model [7–9]. A more accurate model based on FEA using dual moisture transport mechanisms has been recently developed for different encapsulation materials [10].

These last calculations were validated experimentally using measurement setup based on miniature temperature and humidity sensors. Using the same sensors [11,12], this work investigates the rates and patterns of moisture ingress into and egress out of PV laminates based on external humidity changes, utilizing measurements at different material depths. The results are compared with depth profiling measurements of the encapsulant inside PV laminates. As shown in Table 1, three laminates were prepared using two types of backsheets and two different lamination processes resulting of different degrees of crosslinking (DoC). The moisture ingress was measured during DH and UV-DH combined exposure tests. This last combined test aims at more realistic representation of degradation by simulating multiple factors simultaneously [13].

2 EXPERIMENTAL PART

2.1 Sample preparation

In this study, three laminates were assembled. The following components were used (see Table 1):

- Two different PET-based backsheets (BSs) from different manufacturers
- Four layers of EVA from same manufacturer and one glass plate for each laminate
- Flexible sensor strips with 4 humidity sensors for each laminate

Three of the sensors were laminated between the EVA layers at different distances from the BS and the fourth was left outside the laminate for air humidity measurement **(**

Figure 1**)**. Sensor #1 was placed between the EVA and the glass, #2 was laminated in the middle of the sample between two EVA layers on each side and #3 was installed between the EVA and the BS. Since the moisture enters perpendicular to the BS surface, the lateral displacement of the sensors does not affect the humidity concentration [11].

Table 1 Different setup of the lamination and backsheet type used

Laminates	#a	#b	#c
Backsheet	TPT	CPC	TPT
Lamination (t)	10 min	10 min	5 min
DoC (%)	High	High	Low
Water vapor transmission (WVTR)	0.7g/m^2.d 23°C/85% RH	3.9g/m^2.d 38°C/90% RH	0.7g/m^2.d 23°C/85% RH

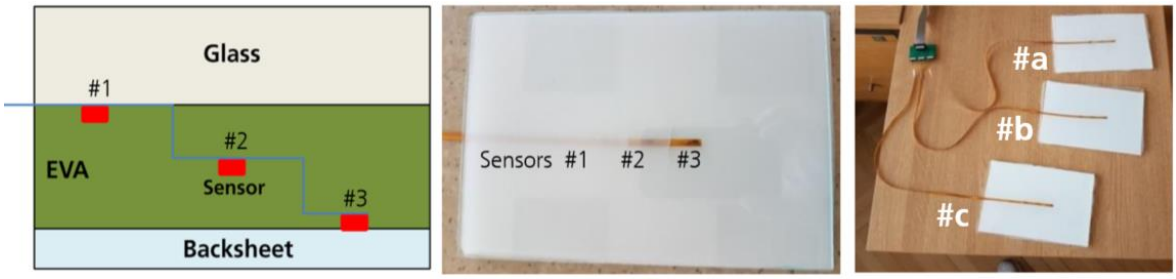

Figure 1 Schematic representation of the sensors positions in the laminate. Middle: Overview of the components used for assembling the laminates before adding the backsheet. Right: Assembled samples after lamination with an external digital acquisition reader

The sensor strips containing miniature temperature (T) and relative humidity (RH) sensors are encapsulated in various laminates. The sensors used are Sensirion SHT-25 and SHT-W2. Both have been shown to be resistant to the high temperature and able to measure the humidity in the encapsulant accurately [12]. The strips are connected to a printed circuit board (PCB) containing the necessary readout electronics. Custom software is used to evaluate the measurement results.

2.2 Accelerated aging

During the DH aging, for three constant temperatures (T) (40, 60, 85 °C), the relative humidity (RH) in the climatic chamber was varied as shown in Figure 2**.** The RH was kept constant until equilibrium of the sensors was reached.

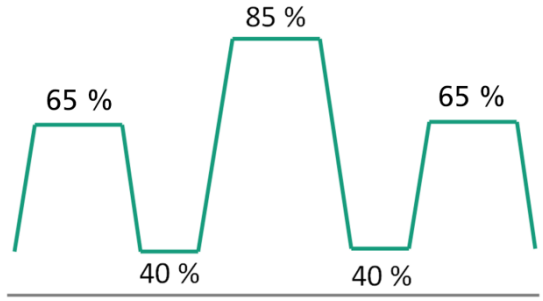

Figure 2 RH cycle for each constant temperature

During the combined UV-DH aging, the samples were subjected to a UV irradiation around 160 W/m^2 - air 85 % RH / 60 °C. Due to the UV irradiation, the sample conditions were around 60 % RH at 75 °C.

3 RESULTS AND DISCUSSION

3.1 Moisture monitoring during Damp Heat tests

Figure *3* shows an example of the measured RH of all positions inside the laminates and one outside during the RH cycle applied in the chamber. As expected, the sensor encapsulated closer to the glass (pos. #1) detects the moisture ingress and egress with a larger delay than the sensor embedded closer towards the backsheet. Furthermore, the water uptake inside the laminate describes a reversible behavior for all sensors positions at 85°C.

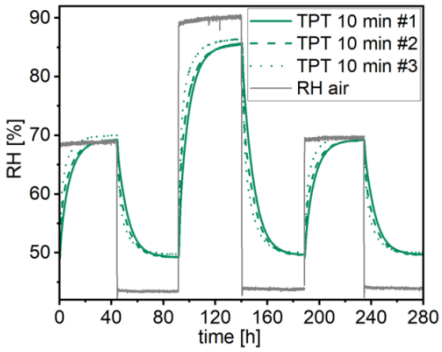

Figure 3 Measured moisture ingress in laminate #a for RH cycle at 85 °C

Backsheet effect

All sensors showed higher RH values by using CPC backsheet (Figure 4). The equilibrium is reached faster, after ~15 h using CPC and after ~32 h using TPT. This behavior indicates a higher diffusion rate through the backsheet as indicated by the higher WVTR (see Table 1)

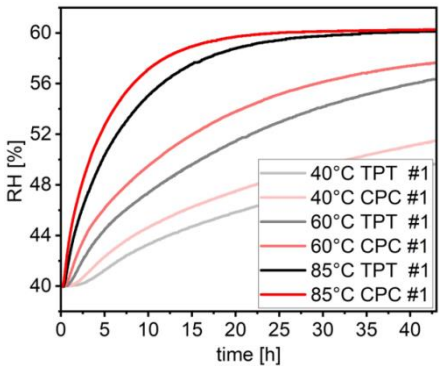

Figure 4 Measured moisture ingress in laminates #a and #b at different constant temperature

Since the data were acquired at three different temperatures, the effective activation energy (E_A) was determined assuming an Arrhenius-like behavior Eqn. (1)

$$D = D_0 \cdot \exp(-E_A/RT) \quad (1)$$

Where D is the diffusion coefficient, D_0 is a factor gathering various constants as well as entropy considerations, E_A is the activation energy commonly expressed in J/mol, R is the universal gas constant (8.314 J mol^{-1} K^{-1}) and T is the temperature in K.

$$D = A \exp(-E_A/RT)\,[H_2O] \quad (2)$$

$$D = A \exp(-E_A/RT)\, RH \exp(-H_s/RT) \quad (3)$$

$$D = A \exp(-E_A^{eff}/RT)\, RH \quad (4)$$

$$\mathrm{Ln}(D) = -E_A^{eff}/RT + \mathrm{Ln}(A) + \mathrm{Ln}(RH) \quad (5)$$

The concentration of water in a polymer at a given temperature is equal to the product of saturation solubility S and the relative humidity: $[H_2O] = S*RH$ [14]. The solubility usually is proportional to an Arrhenius-like expression where E_A is replaced by the enthalpy of solvation Hs allowing **Eqn. (2)** to be expressed as **Eqn. (3).** The two empirically determined values of activation energy and solubility enthalpy can be combined and expressed as effective activation energy (E_A^{eff}) to give **Eqn. (4).** The E_A^{eff} summarizes the diffusion properties. It is important to note that the key parameter is relative humidity at the sample temperature, not the vapor pressure of water.

Figure *5* shows the Arrhenius plots for all sensors of the laminates #a, #b and #c, where y-axes specifies the time required to reach the equilibrium in RH. The corresponding temperature is indicated on the x-axes (**Eqn. (5)**).

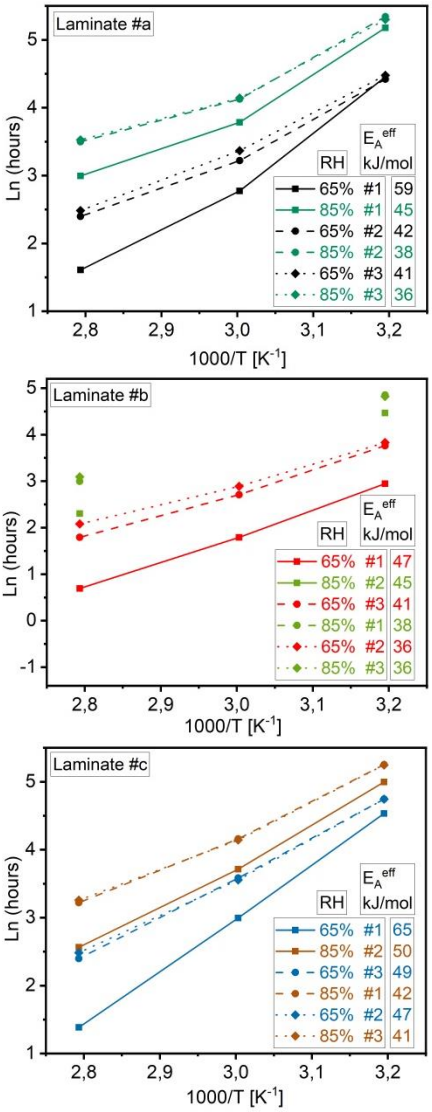

Figure 5 Arrhenius plots describing the rate of moisture ingress during damp-heat aging. The calculated E_A^{eff} are presented for each RH setting

Using different backsheet types between laminate #a and #b (Figure *6*), the E_A^{eff} presented in Figure *5* showed lower values at 65% RH for laminate #b, which confirm the higher water vapor transmission rates in Table 1 taken from the datasheet.

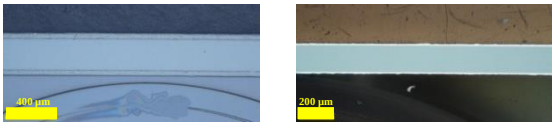

Figure 6 Digital microscopy images of the cross-section of the two backsheets used in the study

Lamination condition effect

The diffusion seems to exhibit dependence on the lamination time **(**Figure 7**);** due to different degree of cross-linking of the EVA [3,15]. More precisely, the laminate with partially crosslinked EVA (laminate #c) showed slower moisture ingress (higher E_A^{eff} values Figure *5*) at all sensor positions.

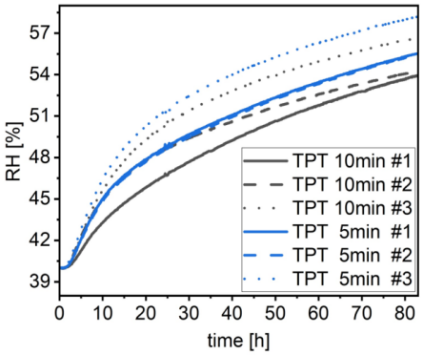

Figure 7 Measured moisture ingress in laminate #a and #c at 40 °C, 65 % RH

During the lamination, the EVA curing process results in the consumption of crosslinking additives. Crosslinking or branching interconnects the polymer chains and reduces its crystallinity [16]. Therefore, a short lamination results in a weakly crosslinked EVA which has a higher degree of crystallinity. The dense packaging of the EVA in the crystallites acts as a diffusion barrier for the moisture ingress, which consequently, reducing the speed of diffusion through the material [17]**.**

3.2 Moisture monitoring during UV-DH combined test

To visualize the pathway of moisture during UV-DH combined test, the moisture and the temperature in the encapsulant is plotted at the three various depths for both laminates #a and #b, as shown in Figure 8 and Figure 9.

In the beginning, all sensors show same initial RH value. As the chamber humidity drops (e.g. at around 30 hours), The diffusion of moisture through backsheet and EVA changes strongly, the sensor in pos. #3 shows a decrease in moisture as expected, while the sensor in pos. #1 shows an unexpected rise in relative humidity. For both laminates (#a and #b), the RH values close to the backsheet change quickly with the environmental conditions. The reasons for this behavior is still up for discussion to this date.

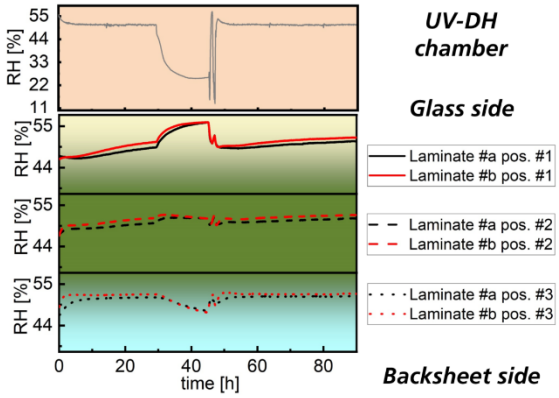

Figure 8 Measured moisture ingress in laminate #a and #b during UV-DH at ~ 160 W/m^2 - air 60 % RH / 75 °C

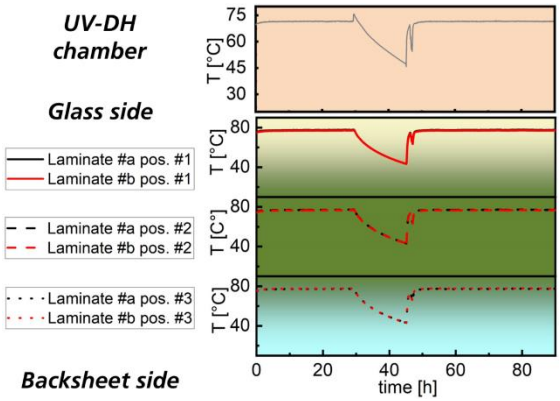

Figure 9 Measured temperature in laminate #a and #b during UV-DH at ~ 160 W/m^2 - air 60 % RH / 75 °C

4 SUMMARY

A comparison of the effect of the backsheet permeability and degree of crosslinking of the EVA on (a) initial moisture uptake and (b) time required for saturation are presented. This shows the importance of material properties and therefore material choice when making lifetime predictions. The periods at various RH and temperatures can be related back to reference conditions if the kinetics is known, specifically, the activation energy and the kinetic order of the moisture diffusion. The results demonstrate differences in diffusion rate in dependence of the backsheet type as well as degree of crosslinking of the encapsulant. A slower moisture ingress and lower effective activation energy (E_A^{eff}) could be obtained for the encapsulation with a lower degree of crosslinking. Furthermore, during the combined UV-DH seems to generate opposite pathways of diffusion between the sensor positions near the glass and near the backsheet before the equilibrium. These findings are up to discussion and have to be locked upon in more detail in future investigations.

ACKNOWLEDGEMENTS

This work was funded by the European Union's Horizon 2020 research and innovation program in the framework of the project "Solar-Train" under the Marie Sklodowska-Curie GA 721452—H2020MSCA-ITN-2016.

References

[1] A. Morlier, S. Klotz, S. Sczuka et al., "Influence of the Curing State of Ethylene-Vinyl Acetate on Photovoltaic Modules Aging," 2013.

[2] S. Jonai, K. Hara, Y. Tsutsui et al., "Relationship between cross-linking conditions of ethylene vinyl acetate and potential induced degradation for crystalline silicon photovoltaic modules," *Japanese Journal of Applied Physics*, vol. 54, 8S1, 08KG01, 2015.

[3] G. Oreski, A. Rauschenbach, C. Hirschl et al., "Crosslinking and post-crosslinking of ethylene vinyl acetate in photovoltaic modules," *Journal of Applied Polymer Science*, vol. 134, no. 23, p. 101, 2017.

[4] M. Koentges, S. Kurtz, C. Packard et al., "Performance and Reliability of Photovoltaic Systems. Subtask 3.2: Review of Failures of Photovoltaic Modules," Agency, International Energy, 2014.

[5] M. Koentges, G. Oreski, U. Jahn et al., "Assessment of photovoltaic module failures in the field: Report IEA-PVPS T13-09:2017," IEA International Energy Agency, 2017, http://iea-pvps.org/index.php?id=435.

[6] A. Masuda, N. Uchiyama, and Y. Hara, "Degradation by acetic acid for crystalline Si photovoltaic modules," *Japanese Journal of Applied Physics Part 1-Regular Papers Brief Communications & Review Papers*, vol. 54, 4S, 04DR04, 2015.

[7] P. Huelsmann, M. Heck, and M. Koehl, "Simulation of water vapor ingress into PV-modules under different climatic conditions," *Journal of Materials*, vol. 2013, 7 pages (1-7?), 2013.

[8] M. D. Kempe, "Modeling of rates of moisture ingress into photovoltaic modules," *Solar Energy Materials and Solar Cells*, vol. 90, no. 16, pp. 2720–2738, 2006.

[9] S. Mitterhofer, M. Jankovec, and M. Topic, "One- and two-dimensional finite element analysis of humidity ingress in polymeric materials," *in Proc. 54th Int. Conf. Microelectron., Devices Mater.*,, 2018, pp. 93–98.

[10] S. Mitterhofer, C. Barretta, L. F. Castillon et al., "A Dual-Transport Model of Moisture Diffusion in PV Encapsulants for Finite-Element Simulations," *IEEE Journal of Photovoltaics*, vol. 10, no. 1, pp. 94–102.

[11] M. Jankovec, F. Galliano, E. Annigoni et al., "In-Situ Monitoring of Moisture Ingress in PV Modules Using Digital Humidity Sensors," *IEEE Journal of Photovoltaics*, vol. 6, no. 5, pp. 1152–1159, 2016.

[12] M. Jankovec, K. Brecl, J. Kurnik et al., "Evaluation of different temperature measurement methods of crystalline silicon PV modules," in *Proceedings of the 25th European Photovoltaic Solar Energy Conference and Exhibition/ 5th World Conference on Energy Conversion*, pp. 4257–4260, 2010.

[13] D. E. Mansour, C. Barretta, L. Pitta Bauermann et al., "Effect of Backsheet Properties on PV Encapsulant Degradation during Combined Accelerated Aging Tests," *Sustainability*, vol. 12, no. 12, p. 5208, 2020.

[14] J. E. Pickett and D. J. Coyle, “Hydrolysis kinetics of condensation polymers under humidity aging conditions,” *Polymer Degradation and Stability*, vol. 98, no. 7, pp. 1311–1320, 2013.
[15] C. Herzog, T. Müller, M. Heinrich et al., “Differential Scanning Calorimetry for Simulation and Optimization of the Lamination Process,” 2019.
[16] A. P. Patel, A. Sinha, and G. Tamizhmani, “Field-Aged Glass/Backsheet and Glass/Glass PV Modules: Encapsulant Degradation Comparison,” *IEEE Journal of Photovoltaics*, vol. 10, no. 2, pp. 607–615, 2020.
[17] C. Hirschl, M. Biebl-Rydlo, M. DeBiaso et al., “Determining the degree of crosslinking of ethylene vinyl acetate photovltaic module encapsulants - A comparative study,” *Solar Energy Materials and Solar Cells*, vol. 116, no. 2013, pp. 203–218, 2013.